P-141 NMR structure refinement by torsion angle molecular dynamics simulation using a physical force field in CYANA

Teppei Ikeya[1], Masaki Mishima[1], Yutaka Ito[1] and Peter Güntert[2,3,4]

[1] Graduate School of Science, Tokyo Metropolitan University, Tokyo
[2] Center for Priority Areas, Tokyo Metropolitan University, Tokyo
[3] Institute of Biophysical Chemistry, Goethe-University Frankfurt, Frankfurt am Main, Germany
[4] Frankfurt Institute of Advanced Studies, Goethe-University Frankfurt, Frankfurt am Main, Germany

ABSTRACT

Torsion angle molecular dynamics (TAMD) is widely used for NMR structure calculation. It is more robust, allows longer step-sizes than in Cartesian space, and can quickly accomplish the tertiary structure with angle and distance restraints. The program CYANA adopting TAMD can efficiently calculate NMR structures with automated NOE assignment, but it is not trivial to refine these structures by TAMD since the physical energy in torsion angle space is not identical to the one in Cartesian space. We show a new TAMD implementation in CYANA and its feasibility for protein structure refinement.

INTRODUCTION

Torsion angle molecular dynamics (TAMD) is a standard tool for NMR structure calculation. It reduces the number of degrees of freedom and permits longer step-sizes than in Cartesian space where stiff degrees of freedom (bond lengths and angles) result in high frequency motions. However, some well-known issues make TAMD applications difficult. The van der Wall repulsion between atoms through "1-4","1-5", and "1-6" covalent contacts are not relaxed in the torsion angle representation and result in unrealistically high energy regions on the energy surface of a molecule. In addition, it is not trivial in TAMD to treat a complicated system with an enormous number of molecules like a model including thousands of waters. Thus, TAMD was not utilized for simulations of various molecules and long time-scales such as protein folding which is susceptible to fairly small differences of the energy potential. However, the distortion is limited exclusively to certain areas of the energy surface far from the local minima in the φ,ψ dihedral angle energy map that are characteristic for secondary structures (Fig 1). It was not cleared whether TAMD with a physical potential is sufficient for NMR structure refinement that is potentially robust to small distortions of the force field because of the support from distance and angle restrains derived from NMR data. Thus, comprehensive studies are prerequisite to assess the validity of force fields in TAMD, and to confirm its feasibility for the structure refinement. Recently we transferred a physical force filed, the Amber potential, into the program CYANA adopting TAMD, and

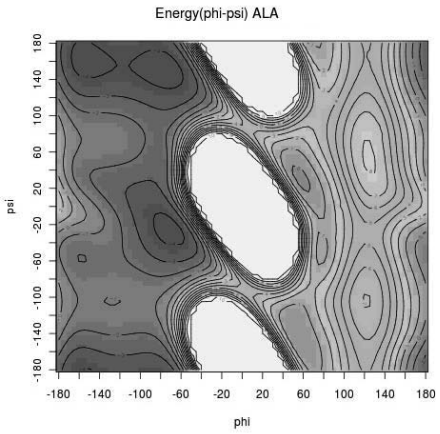

Fig. 1 φ,ψ dihedral angle energy map of alanine. Dark and light colors show lower and higher energy areas. The regions around φ = 0° have extremely high energy, while the local minima in the φ range -180 to -40°, which contribute to secondary structure, are well conserved.

Molecular Dynamics, structure refinement, CYANA

implemented a numerical calculation method and an implicit water model that makes a target molecule independent from the solvent. Here we evaluate the physical force field in TAMD with CYANA for NMR protein structure refinement.

● METHODS

The Amber ff03 potential energy function was implemented with a Generalized Born implicit water model into CYANA 3.0. A predictor-corrector method was employed for molecular dynamics, which is of a higher order than the leap-frog scheme currently used in CYANA. For energy minimization, a quasi-Newton method was adopted instead of the conjugate gradient method of CYANA, which can circumvent local energy obstacles more efficiently .

35 test protein structures from the Protein Data Bank (PDB) are chosen for the evaluation of the current force field in TAMD, in which any two have a sequence homology below 25%. Metal-binding, membrane and oligomeric proteins, proteins having chain breaks in the middle of the sequence, and highly extended structures were excluded. Decoys for each protein, i.e. non-native structures but including near-native ones, are generated performing short molecular dynamics simulations with randomly created different number of restraints using the conventional CYANA. Those structures are optimized under the physical force field, and evaluated by comparing the root mean square deviation (RMSD) to the reference structures.

Another 14 proteins that were targets of CASD-NMR, a critical assessment of automated structure determination by NMR, are used for the test of the energy refinement after the structure calculations with a conventional CYANA target function as well as automated NOESY assignments.

● RESULTS

Figure 2 plots the energies of 1501 obtained structures including the native one. Strong correlations are clearly seen, particularly in the near-native structures with RMSD less than 10 Å, although some structures that are far from the native one have lower energies. This suggests that the current force field is sufficient for obtaining refined structures from almost globally folded ones, but not from entirely different folds.

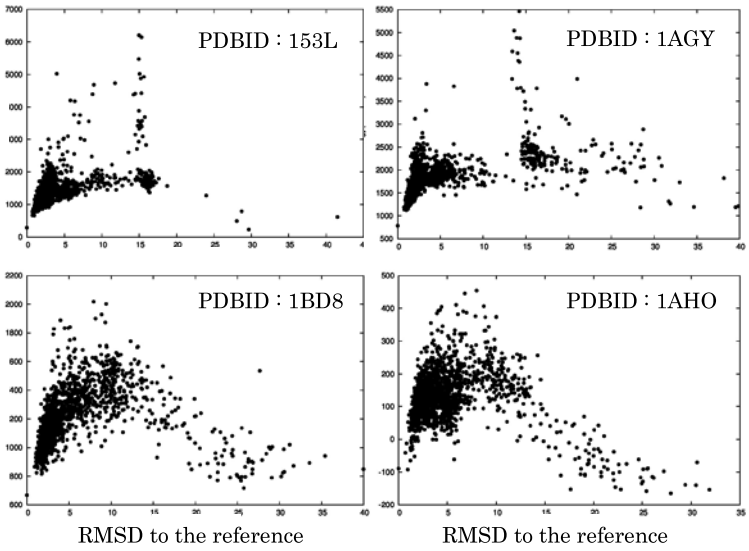

Fig. 2 Optimized energies for the native and all decoy structures plotted against the RMSD to the reference structure. Strong correlations can be seen in the range 0–10 Å.

The energy refinement of the CASD structures is carried out with conventional simulated annealing and a replica exchange method in CYANA. It shows that most validation scores of the structures, i.e., Ramachandran plot, ratio of secondary structure, packing quality, rotamer normality, etc., are improved compared to those obtained with our conventional Cartesian optimization program, OPALp.

● REFERENCES

1) Chen J., Im W., Brooks C.L.III, Applicaftion of Torsion Angle Molecular Dynamics for Efficient Sampling of Protein Conformations, *J.Comp.Chem*. 26, 1565-1578 (2005)

2) Katritch V., Totrov M., Abagyan R., ICFF: A New Method to Incorporate Implicit Flexibility into an Internal Coordinate Force Field, *J.Comp.Chem*. 24, 254-265 (2002)

P-142 Substructure search using two types of matching of bipartite graphs associated with NMR chemical shift data

Shungo Koichi[1], Hiroyuki Koshino[2] and Hiroko Satoh[3]
[1]Department of Systems Design and Engineering, Nanzan University
[2]RIKEN Advanced Science Institute, and
[3]National Institute of Informatics.

ABSTRACT

In database-oriented chemical structure elucidation, structures are usually predicted with substructures selected from a database using 1D NMR data as a query. Exhaustive and minimal search of relevant substructures efficiently leads to a correct structure. We developed two methods of substructure search. One uses the convex bipartite matching (CBM) and the other employs the weighted bipartite matching (WBM). The method with WBM always retrieves a substructure selected by the method with CBM. This hierarchic search provides an exhaustive and minimal search. We will describe the two search methods.

1. Introduction

As automatic chemical structure elucidation systems from NMR data, various systems including DENDRAL, CHEMICS, SpecInfo, KnowItAll, and "ACD/Structure Elucidator" ([1]-[12]) are proposed and getting widely used. However, in some cases, particularly in the case of a complex compound, solutions of those systems have not satisfied the user yet. And so, establishing an automatic chemical structure elucidation system is still a great challenge in the computational chemistry. In order to overcome the challenge, we have been developing a database-oriented chemical structure elucidation system from 1D NMR data including an NMR chemical shift prediction system CAST/CNMR together with new canonical coding ([13]-[18]).

The database of the system consists of chemical structures associated to experimental ^{13}C NMR chemical shifts data. With a query 1D NMR data, the system first retrieves substructures with NMR data similar to the query. Then, the system elucidates a chemical structure by identifying overlap parts of the retrieved substructures. As long as we adopt this procedure, retrieving substructures is one of the critical steps. If an essential substructure is not selected, we never obtain a correct chemical structure due to the absence of the essential part of the structure. Therefore, it is important to establish a method to search all substructures needed for the elucidation to be completed.

However, if the number of retrieved substructures is huge, it takes high computational cost to elucidate a structure because the number of candidate structures is exploded. In the worst case, it is impossible to complete the elucidation within realistic time. Thus, it is necessary to develop an efficient algorithm for an exhaustive and minimal search of relevant substructures. Aiming to this type of search, we developed two search methods using two types of bipartite matching algorithm. These algorithms are well known in the contexts of combinatorial optimization and graph algorithm. The first method utilizes the convex bipartite matching (CBM) algorithm, and the second one employs the weighted bipartite matching (WBM) algorithm.

Keywords: Substructure search, Bipartite graph matching, Structure elucidation

The first method is faster than the second one. However, its criterion to judge the similarity of NMR data is severer than that of the second one. Hence, in some cases, the result of search can be narrower than we expected. On the other hand, the second method is slower than the first one. However, its criterion of the similarity of NMR data is laxer than that of the second one. In fact, the second method always retrieves any substructure selected by the first one. With the aid of these properties, we achieved an exhaustive and minimal search of relevant substructures.

2. Two Search Methods

Before we describe the two methods, we introduce some notations. Let $G = (U, V; E)$ be the bipartite graph with a left vertex set U, right vertex set V and edge set E. An edge e in E is a pair of a vertex u in U and vertex v in V. A matching M is a subset of E whose edges do not share a vertex. A vertex x of G is called covered by a matching M if M has an edge e that contains x. In the following, the left vertex set U corresponds to a query 1D NMR data, which is assumed to be a set of NMR chemical shifts.

The object of the search is limited to a certain type of substructure; a substructure has a central atom and the other atoms in the substructure are connected within a user-designated number of bonds from the central atom. The central atom is called here a target atom. Since structures in the database are associated to NMR chemical shifts, the system obtains, from a substructure, a set of NMR chemical shifts assigned to its atoms. The right vertex set V corresponds to this set of NMR chemical shifts. A basic difference between the two methods is how we define the edge set E.

In the first method, we set an edge $e=(u, v)$ in E if the (absolute) difference $|u-v|$ between NMR chemical shifts u and v is less than or equal to a user-designated allowance a. It is known that a bipartite graph defined in this way is a convex bipartite graph. Using the CBM algorithm, we can efficiently compute a maximum matching M, which has the maximum number of edges among all matchings in G. If the number of edges in M is equal to either the size of U or that of V, then we say that the target atom in a substructure is hit, and in this case, a matching M gives a correspondence between the query NMR chemical shifts and those for a substructure. Note here that the difference of each pair in the correspondence is at most the user-designated allowance a.

In the second method, we define E to be the set of all pairs of an NMR chemical shift in U and NMR chemical shift in V. And, we give a weight w_e to each edge $e=(u, v)$ in E, where w_e is set to be the (absolute) difference $|u-v|$ between the NMR chemical shifts u and v. In this way, we obtain a weighted bipartite graph. Using the WBM algorithm, we can efficiently compute the minimum weighted matching W, which has the minimum weight among all matchings that covers U or V in G, where the weight is given by the sum of the weights w_e on edges e in W. If the weight of W is less than or equal to a user-designated allowance a times the minimum of the sizes of U or V, then we say that the target atom in a substructure is hit. In this case, a minimum weighed matching W also gives a correspondence between the query NMR chemical shifts and those for a substructure. In fact, the average of the differences of pairs in the correspondence is less than or equal to the user-designated allowance a. Therefore, the criterion of the second method to judge if the target atom is hit is laxer than that of the first one.

The both methods retrieve substructures with hit target atoms. As you can see, the exhaustiveness of a substructure search by the second method is higher than the first one. However, as mentioned in the introduction, the second method needs more computation time than the first one. Moreover, since the exhaustiveness is inextricably associated with the redundancy, it may be necessary to

remove the non-essential substructures from the search results. Hence, the two methods play roles complementarily.

3. Illustrative Example.

As a query 1D NMR data, we use a set of NMR chemical shifts: 15.1, 15.5, 17.2, 19.3, 20.7, 27.1, 28.1, 36.8, 37.4, 38.8, 40.3, 51.5, 54.9, 78.4, 81.0, 99.4, 100.3, 123.6, 127.6, 132.8, 146.6, 151.0, 155.5, 162.8, and 164.0 [19]. An example of a substructure is shown in Figure 1. The substructure consists of the atoms within three bonds from a target atom as in Figure 1. Each of the numbers besides the atoms is the reported NMR chemical shift for the corresponding atom. This substructure is characterized by a set of NMR chemical shifts: 15.6, 18.4, 27.2, 28.1, 37.1, 38.5, 38.8, 55.3, and 79.0. A user-designated allowance *a* is set to be 0.45. The convex bipartite graph used in the first method is shown in Figure 2. Some of the data are not shown in Figure 2 for simplicity. The bold lines mean that those chemical shifts are matched in the maximum matching of the convex bipartite graph. In this case, the number of pairs of NMR chemical shifts matched in the maximum matching is smaller than the number of atoms of the substructure. Therefore, the target atom is not hit, or the substructure is not submitted to the search process of the first method, either.

Figure 3 shows the minimum weighted matching obtained with the second method. The sum of the weight values of this matching is equal to 3.5. This is smaller than the use-designated allowance times the number of atoms of the substructures: 0.45 x 9 = 4.05. Therefore, the substructure is selected with the second method. As the final results, the substructures shown in Figures 1 and 4 are output. By identifying the overlap parts of these substructures, they cover the structure as shown in Figure 5, which is exactly the structure reported in [19]. This is an example, demonstrating that the second method works to elucidate a structure. Although we do not show here, there are other cases where the first method plays an important role.

The user can add the type of carbons (primary, secondary, tertiary and quaternary carbon atoms) to the query, and the system can utilize it.

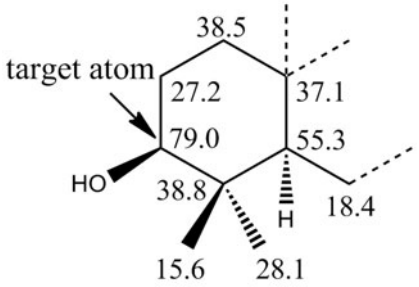

Figure 1. A substructure.

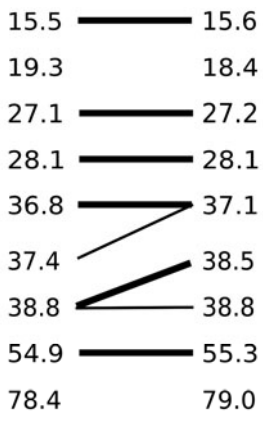

Figure 2. A convex bipartite graph and its maximum matching (bold lines).

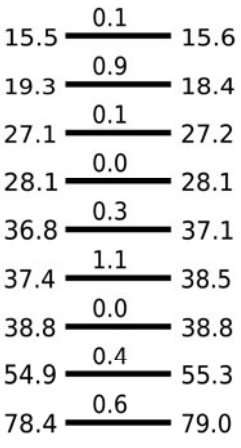

Figure 3. The minimum weighted matching.

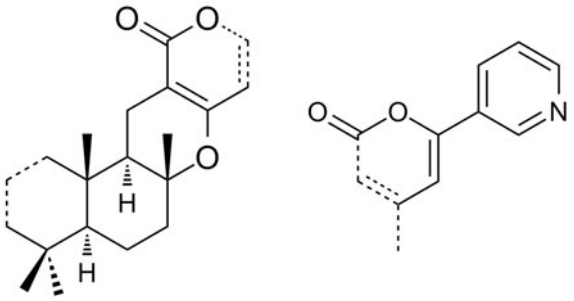

Figure 4. Substructures.

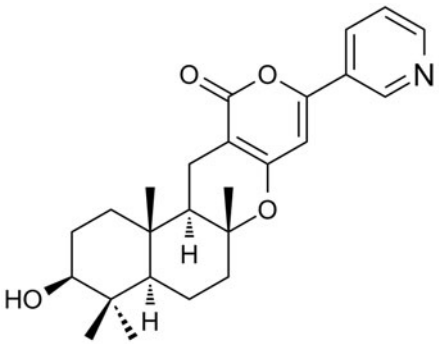

Figure 5. An elucidated chemical structure.

4. Conclusion

In the first step of development of a structure elucidation system using 1D NMR data, we developed two methods for searching relevant substructures. These two methods utilize convex bipartite matching (CBM) and weighted bipartite matching (WBM), respectively. The method with WBM always gives substructures including the results from the method with CBM but requires high computational cost compared to the method with CBM. By combining these methods, the user will reach the correct structure efficiently.

References

[1] Duffield, A. M.; Rovertson, A. V.; Djerassi, C.; Buchanan, B.G.; Shtherland, G. L.; Feigenbaum, E. A.; Lederberg, J., *J. Am. Chem. Soc.* **1969**, *91*, 2977.

[2] Funatsu, K.; Sasaki, S., *J. Chem. Inf. Comput. Sci.* **1996**, *36*, 190**.**

[3] Bremser, W., *Angew. Chem. Int. Ed. Engl.* **1988**, *27*, 247.

[4] Will, M.; Fachinger, W.; Richert, J. R., *J. Chem. Inf. Comput. Sci.* **1996**, *36*, 221.

[5] Advanced Chemistry Development, Inc. http://www.acdlabs.com

[6] Bio-Rad Laboratories Inc. http://www.bio-rad.com

[7] Schütz, V.; Purtuc, V.; Felsinger, S.l Robien, W., *Fresen. J. Anal. Chem.* **1997**, *359*, 33.

[8] Seger, C.; Jandl, G.l Brader, G.l Robien, W.; Hofer, O.; Greger, H., *Fresen. J. Anal. Chem.* **1997**, *359*, 42.

[9] Lindel, T., Junker, J., Köck, M., *Eur. J. Org. Chem.* **1999**, *3,* 579.

[10] Masui H.; Hong H., *J. Chem. Inf. Model.* **2006**, *46*, 775.

[11] Meiler, J.; Will, M., *J. Chem. Inf. Comput. Sci.* **2001**, *41*, 1535.

[12] Meiler, J.; Sanli, E.; Junker, J.; Meusinger, R.; Lindel, T.; Will, M.; Maier W.; Köck, M., *J. Chem. Inf. Comput. Sci*. **2002**, *42*, 241.

[13] Satoh, H.; Koshino, H.; Funatsu, K.; Nakata, T., *J. Chem. Inf. Comput. Sci.* **2000**, *40*, 622.

[14] Satoh, H.; Koshino, H.; Funatsu, K.; Nakata, T., *J. Chem. Inf. Comput. Sci.* **2001**, *41*, 1106.

[15] Satoh, H.; Koshino, H.; Nakata, T., *J. Comput. Aided Chem.* **2002**, *3*, 48.

[16] Satoh, H.; Koshino, H.; Uzawa, J.; Nakata, T., *Tetrahedron* **2003**, *59*, 4539.

[17] Satoh, H.; Koshino, H.; Uno, T.; Koichi, S.; Iwata, S.; Nakata, T., *Tetrahedron,* **2005**, *61*, 7431.

[18] Koichi, S.; Iwata S.; Uno, T.; Koshino H.; Satoh H., *J. Chem. Inf. Model.* **2007**, *47*, 1734.

[19] Itoh, T.; Tokunaga, K.; Matsuda, Y.; Fujii, I.; Abe, I.; Ebizuka, Y.; Kushiro, T., *Nature Chemistry* **2010**, *2*, 858.

P-143 CLEAN Processing of Randomly Sampled Multi-Dimensional NMR Data

Junichi Kurita[1], Jun Ashida[1] and Ēriks Kupče[2]

[1]Agilent Technologies Inc., Tokyo, Japan
[2]Agilent Technologies, 6 Mead Rd., Yarnton, Oxford, OX5 1QU, UK

ABSTRACT. We show that the CLEAN processing [1] that originally was introduced for reconstructing multidimensional spectra from projections is also useful for processing randomly sampled data sets. The technique was tested using randomly sampled 2D and 3D liquids and solids spectra. The time saving factor of 5 to 6 was achieved in 2D applications while in 3D experiments a factor of 20 to 30 is readily achievable.

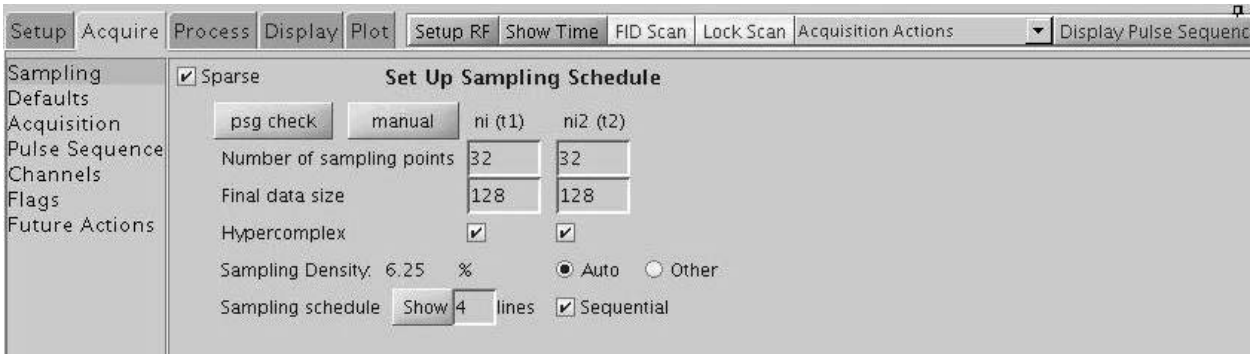

Fig. 1. The GUI acquisition panel for random sampling in VNMRJ.

The user interface for setting up experiments with random sampling is shown in Fig. 1. It permits both automatic setup using the standard sampling schedule generator as well as use of the user defined sampling schedules. The sparsity level is defined by the ratio of the final data size vs the number of sampling points in all dimensions.
Once the data acquisition is finished data can be processed using the user interface of the processing panel (see Fig. 2).

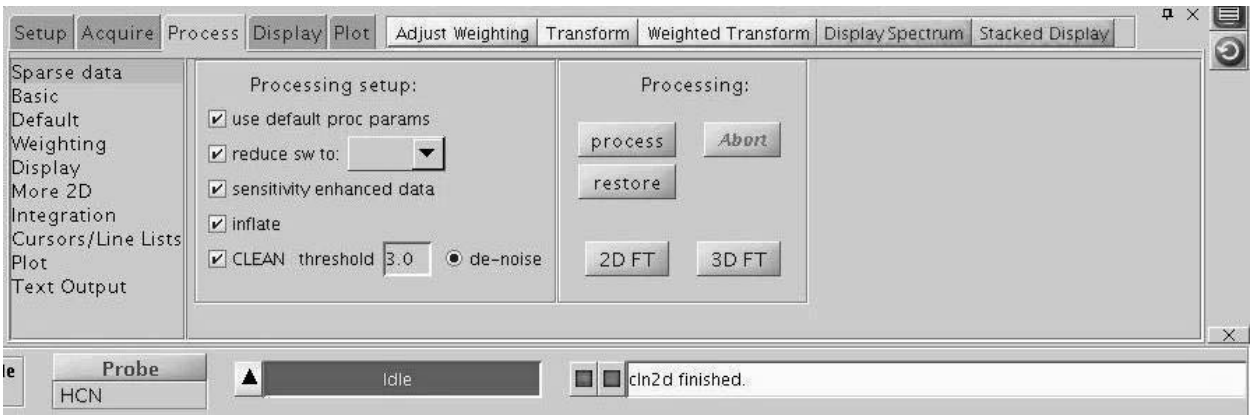

Fig 2. The GUI for the CLEAN processing of randomly sampled data sets in VNMRJ.

An example of CLEAN processing is shown in Fig. 3 for the 3D HNCOCA experiment recorded in 9 hours and demonstrating an exceptional resolution that allows observing both the ^{1}J(CC) and ^{3}J(HH) coupling constants. Further examples are provided for small organic molecules both in liquids and solid state and cover a variety of experiments, such as routine 3D protein backbone assignment experiments and two-dimensional HSQC, HMBC, DQ-COSY, TOCSY and other standard small molecule experiments.

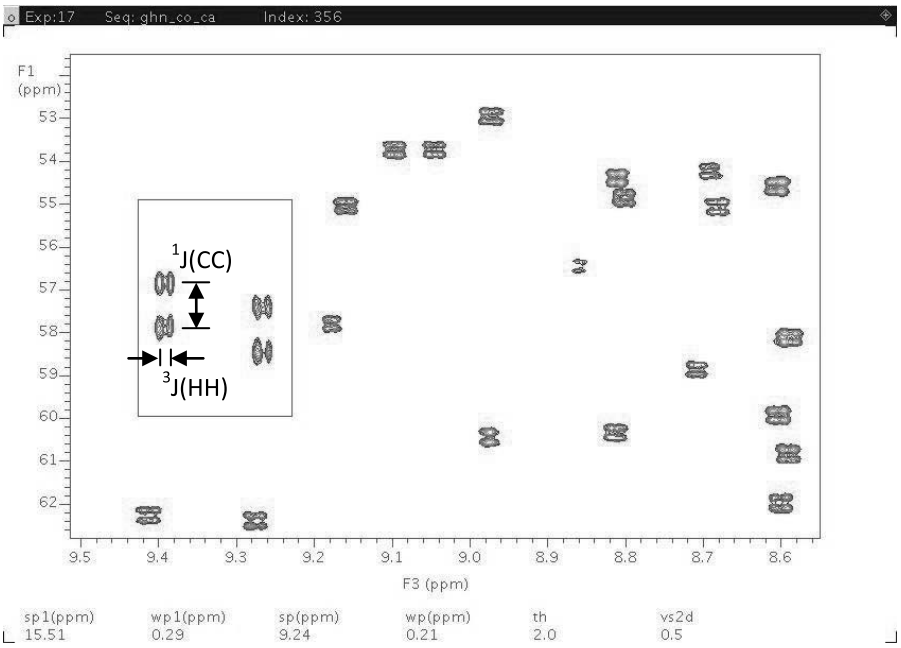

Fig. 3. Screen shot of an ultra-high resolution 3D HN(CO)CA spectrum of 1 mM ubiquitin recorded in ca 9 hours on an Agilent 600 MHz NMR system and processed using the CLEAN algorithm.. The inset shows expanded region of the two peaks in the left bottom corner.

To conclude, the current implementation provides means for routine use of random sampling and CLEAN processing in a variety of standard NMR experiments.

REFERENCES

[5] Ē. Kupče, R. Freeman, *J. Magn. Reson.,* **173,** 317-321 (2006).

Keywords: CLEAN processing, Multi-dimensional NMR, Sparse sampling

P-144 Y

The application of phase-statistical de-noising method to quantitative analysis

Jun Fukazawa[1,2], K. Takegoshi[2], Kazuyuki Takeda[2] and Michio Murata[1,3]
[1]ERATO Lipid Active Structure Project, Graduate School of Science, Osaka University,
[2]Department of Chemistry, Graduate School of Science, Kyoto University and
[3]Department of Chemistry, Graduate School of Science, Osaka University.

In many practical cases, the sensitivity of NMR spectroscopy is low. To improve the signal-to-noise ratio (SNR), it is common to accumulate a number of free induction decays (FIDs). And we recently proposed signal analysis methods for de-noising based on the standard deviation and covariance of the phase of spectra (PSDW and PCW method). They have SNR-better signals than accumulation, but they are lost quantitative information. To revive the quantitation, we designed the improvement of PSDW, to compare the actual PSDW spectra and ideal PSDW spectra.

The sensitivity of NMR spectroscopy is low. In many practical cases, resonance signals in the NMR spectrum are enough smaller than noise and buried in the noise, when the data is acquired only once. To improve the signal-to-noise ratio (SNR), it is common to accumulate a number of free induction decays (FIDs), and we recently proposed signal analysis methods for de-noising based on phase correlation between the NMR signal and the excitation pulse, which is named as phase covariance weighted (PCW) NMR [1,2], and standard deviation of signal's phase, which is named as phase standard deviation weighted (PSDW) NMR [2]. Their applications successfully brought de-noising a noisy spectrum and elimination of spurious signals, for example, the spurious incoherent signal come from the contamination of broadcasting radio waves. But their techniques have a problem. They distort relative intensities of signals favoring larger peaks, and cannot be applied to lineshape analysis or quantitative analysis.

The problem comes from the nonlinearity of the PCW- or PSDW-NMR signals. In this work, we specially studied about PSDW. PSDW signal intensity $S_{\mathrm{PSDW}}(\nu)$ is written as [2]

$$S_{\mathrm{PSDW}}(\nu) = S(\nu) \cdot \left| q_{\sigma_\phi}(\nu) \right|, \quad (1)$$

where $S(\nu)$ is the accumulation signal intensity and $q_{\sigma_\phi}(\nu)$ is the measure of certainty of signal phase and is defined as

$$q_{\sigma_\phi} = 1 - \frac{\sigma_\phi(\nu)}{\overline{\sigma_\phi^N}} = 1 - \frac{\sqrt{3}\sigma_\phi(\nu)}{\pi}, \quad (2)$$

where $\sigma_\phi(\nu)$ is the standard deviation of phase and $\overline{\sigma_\phi^N}$ is the $\sigma_\phi(\nu)$ value for pure noise. Fig. 1 shows the R dependence of the measure of certainty $q_{\sigma_\phi}(\nu)$, where R is a ratio between the pure signal intensity before accumulation $I_0(\nu)$ and the standard deviation of noise intensity σ_I

Phase of signal, PSDW, Quantitation

$(R(\nu) = I_0(\nu)/\sigma_I)$, which represents the SNR at ν. It shows that $q_{\sigma_\phi}(\nu)$ is almost proportional to the R value when R<1 which means that signal is enough weaker than noise.

Fig. 2 shows the signal intensity dependence of PSDW NMR and accumulated NMR. The X-axis is the $S_{\mathrm{PSDW}}/N\sigma_I$, where N is the accumulated spectra number, and Y-axis is R. It shows that the quantitative spectra are revived from the intensity of ideal PSDW spectra by the dotted line function. The function can calculate rigidly but it will be too complicated. Therefore, we approximated the line as

$$R = a\sqrt{x} + b\sqrt[3]{x} + c\sqrt[4]{x}. \quad (3)$$

From the fitting to the data of Fig. 2, (a, b, c) is calculated as (1.79642, -0.34863, 0.17723).

We applied the ideal quantitation reviving method of PSDW spectra to actual PSDW spectra. To examine the de-noising effect, we used the ^{13}C CPMAS experiments spectra data which are carried out by intentionally adding an incoherent noise to the receiver circuit. Fig. 3A and 3B show the normal accumulation spectrum and the spectrum which is applied eq. (3). The asterisk in Fig. 3A is an artificially additional incoherent frequency noise. They show the noise which introduced at 33.2 ppm still exists in normal accumulation was effectively eliminated in new method although the real signals are not distorted. Therefore the new method is a useful technique to eliminate large noises in spectra without distortion of quantitation of spectra.

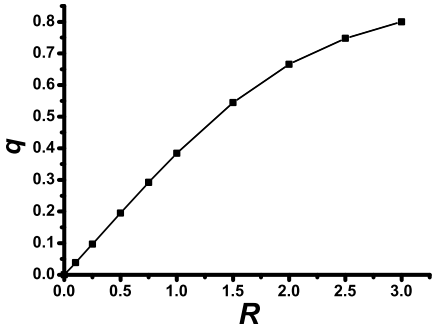

Fig. 1. R dependence of the q_{σ_ϕ}.

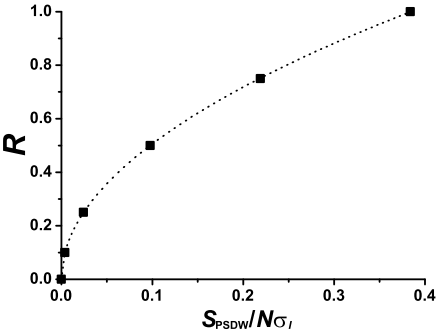

Fig. 2. $S_{PSDW}/N\sigma_I$ dependence of the R. The dotted line is the fitted line which is indicated by eq. (3).

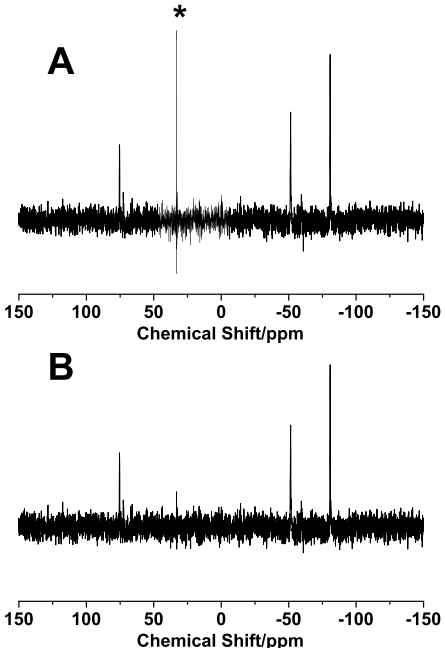

Fig. 3. (A) ^{13}C CPMAS spectra of polycrystalline mixture of glycine and L-alanine measured by adding an additional incoherent frequency signal at 33.2 ppm. (A) The accumulated spectrum. (B) The spectrum which is applied the function of eq. (3). N=1800, and the asterisk indicate the noise at 33.2 ppm.

Reference

[1] J. Fukazawa, K. Takegoshi, Phys. Chem. Chem. Phys., 12 (2010) 11225-11227.

[2] J. Fukazawa, K. Takeda, K. Takegoshi, J. Magn. Reson. 211 (2011) 52-59.

P-145 Y Elemental analysis by NMR

Naoki Ichijo, Kazuyuki Takeda, and K. Takegoshi
Division of Chemistry, Graduate School of Science, Kyoto University

ABSTRACT

We explore the possibility for identifying the composition of atomic elements in materials of chemical interest by NMR. For this purpose, we developed an experimental setup using a cryogen-free, field-variable superconducting magnet, enabling NMR measurements in external fields of up to 7 T. We demonstrate static-field arrayed experiments at a fixed frequency, and show that NMR signals from various nuclear spin species are observed when the carrier frequency matches with the relevant resonance conditions. The quantitative aspect, prospects, and limitations of this approach are also discussed.

1. Introduction

Elemental analysis is an analytical procedure for revealing the composition of atomic elements in an unidentified material of chemical interest. So far, several techniques have been established for this purpose. They include Atomic Absorption Spectrometry (AAS), Electron Probe MicroAnalysis (EPMA), X-ray Photoelectron Spectroscopy (XPS), Inductively Coupled Plasma Atomic Emission Spectroscopy (ICP-AES), and Secondary Ion Mass Spectrometry (SIMS), and so on.

In this work, we explore the feasibility of elemental analysis by NMR spectroscopy. Many of the atomic elements have one or more isotopes possessing spin. Each isotope has a specific gyromagnetic ratio, giving the magnitude of the Zeeman interaction. We aim at judging the existence of the nuclear spin species in the sample of interest from a series of NMR measurements covering their resonance conditions. However, practical difficulty arises with the conventional NMR system using a high-field superconducting magnet. That is, in order to sweep the resonance conditions for a number of spin species, it would be necessary to vary the resonance frequency of the NMR probe; probe re-tuning or replacement would be quite laborious. Even though one manages to do it, quantitative comparison of the signal intensities would be in question.

Instead, we adopted an unconventional option of fixing the carrier frequency and varying the external field. This allows us to observe NMR signals from different spin species without modifying probe tuning. Here, we employ a cryogen-free, field-variable superconducting magnet for this aim. The magnetic field can be varied without consuming helium.

In the following, we describe the principle of NMR elemental analysis, and the experimental setup developed for this purpose. Then, we show demonstrations, and discuss the result.

2. Principle

NMR signals from a nuclear spin species with a gyromagnetic ratio γ are observed under the resonance condition:

$$\omega = -\gamma B_0, \tag{1}$$

Keywords: Elemental analysis, Field sweep

where ω is the Larmor frequency. At a fixed frequency, the relative signal intensity is determined solely by the macroscopic magnetization M of the species. In thermal equilibrium in a magnetic field B_0 and at temperature T, M is represented by the Curie's law as

$$M = \frac{N\gamma^2\hbar^2 I(I+1)B_0}{3k_{\mathrm{B}}T}, \tag{2}$$

where N is the number of the nuclear spins, I is the spin quantum number, k_{B} is the Boltzmann constant.

In this work, we aim at observing NMR signals of various nuclear species with gyromagnetic ratios of γ_i $(i = 1, 2, 3, \ldots)$ in the sample. The external field B_{0i} satisfying the resonance condition is given by

$$B_{0i} = \omega_0/|\gamma_i|. \tag{3}$$

Using eq.(3), we rewrite eq.(2) as

$$\frac{M_i}{\gamma_i I_i(I_i+1)} = \frac{N_i\hbar^2\omega_0}{3k_{\mathrm{B}}T}. \tag{4}$$

It follows that the measured nuclear magnetization, when divided by a factor $\gamma_i I_i(I_i+1)$, should reflect the relative number N_i of the nuclear spins which exist in the sample.

Even though the signal detection sensitivity is common, the nutation rate is proportional to the gyromagnetic ratio γ_i. In order to equate the tilt angles of the pulses for each of the target spin species, either the pulse width or the pulse intensity has to be arrayed together with the external field.

3. Experimental setup

We performed the experiment using a home-built spectrometer[1,2] and a cryogen-free, field-variable superconducting magnet (Cryogenics). This desktop magnet has an external refrigerator to keep the temperature of the magnet wire below 4 K. The magnetic field can be varied between 0 and 7 T by heating a part of the magnet wire, breaking superconductivity, and regulate the electric current flowing through it. When the heater is switched off, the magnet begins to operate in the persistent-current mode again. The static field was controlled automatically by the spectrometer.

The probe, which is also home-made, is equipped with a 3.2-mm spinning module (Chemagnetics). The coil was tuned at 30 MHz. The Q factor was measured to be ca. 40.

4. Results and discussions

We studied aqueous solution of NaH_2PO_4 with a concentration of 6.05 M. The sample was put in a 3-mm glass tube. The signals from ^{1}H ($I = 1/2$), ^{31}P ($I = 1/2$) and ^{23}Na ($I = 3/2$) were expected to be observed. The sample was prepared so that the ratio of the numbers of the spin species was ^{1}H : ^{31}P : ^{23}Na = 20.3 : 1 : 1.

First, we sought the resonance condition for ^{1}H, and then carried out a nutation experiment to calibrate the 90°-pulse width of ^{1}H. Then, we carried out a B_0-arrayed experiment up to 7 T. We found considerable acoustic ringing as increasing the static field. Accordingly, we employed a variation of the Hahn echo sequence with 16-step phase cycling[3]. The pulse width was also arrayed for the reason mentioned above. For the case of ^{1}H, the receiver gain was reduced by 11.0 dB compared to other nuclei, in order to prevent the receiver overload.

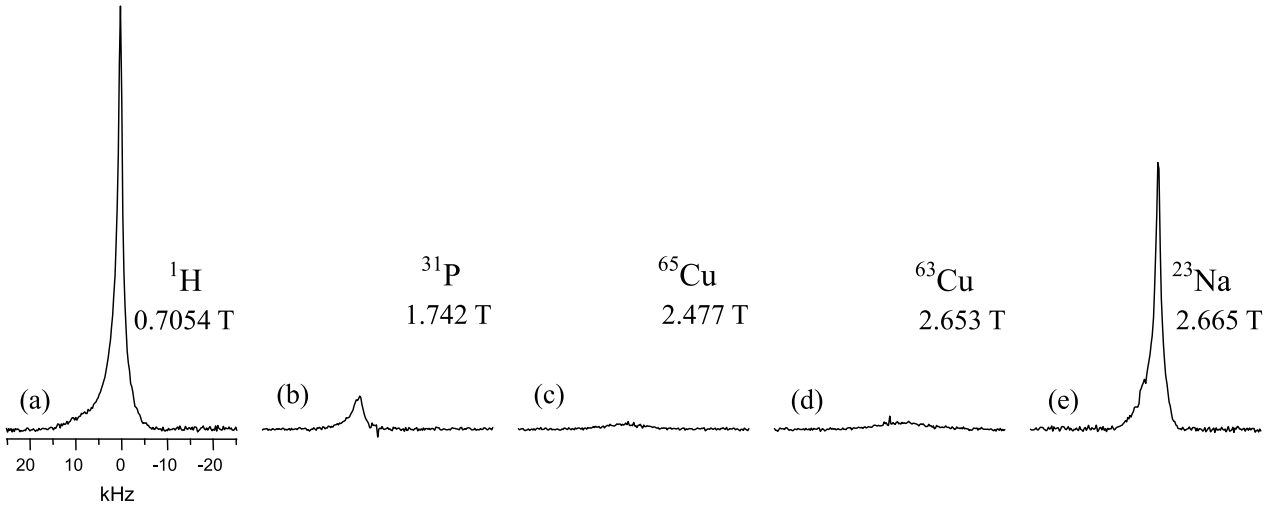

Fig. 1. Spectra obtained in aqueous solution of NaH_2PO_4 in magnetic field of (a) 0.7054 T, (b) 1.742 T, (c) 2.477 T, (d) 2.653 T, and (e) 2.665 T. The carrier frequency was fixed at 30.03 MHz, and the pulse widths were set to 0.8 μs, 1.9 μs, 2.7 μs, 2.9 μs, and 2.9 μs, respectively. The signals were assigned to be ^{1}H, ^{31}P, ^{65}Cu, ^{63}Cu, and ^{23}Na.

Fig. 1(a)-(e) shows spectra of the NMR signals we found in the aqueous solution of NaH_2PO_4. In addition to the signals from ^{1}H, ^{31}P and ^{23}Na, two more signals were detected. They are assigned to be ^{63}Cu and ^{65}Cu contained in the sample coil (see also Table 1). The linewidths of the order of 1 kHz were due to inhomogeneity of the static field in the magnet we used.

Assuming that the peak area intensities reflect the magnetizations, we calculated the relative molar fractions according to eq.(4), by taking the receiver gain into account. The result was ^{1}H : ^{31}P : ^{23}Na = 28.5 : 1 : 1.12. The discrepancy with the actual ratio was ascribed to the decoherence effect during the Hahn echo sequence.

In order to verify this, we performed the CPMG sequence. This allows us to extrapolate the signal intensity to just after the first 90° pulse. In addition, the sensitivity attained per experimental time was improved. As demonstrated in Fig. 2, the spin-spin relaxation times of these three species were not the same. By extrapolating the data, we obtained the ratio ^{1}H : ^{31}P : ^{23}Na = 19.3 : 1 : 0.963. Compared with the result acquired by the Hahn echo, more accurate evaluation could be made. Fig. 3 shows the histogram of the relative abundance of ^{1}H, ^{31}P and ^{23}Na based on the extrapolated values.

Table 1. Gyromagnetic ratios.

Isotope	$\gamma / 2\pi$ [4] / (MHz T^{-1})
^{1}H	42.5774
^{31}P	17.237
^{65}Cu	12.089
^{63}Cu	11.285
^{23}Na	11.262

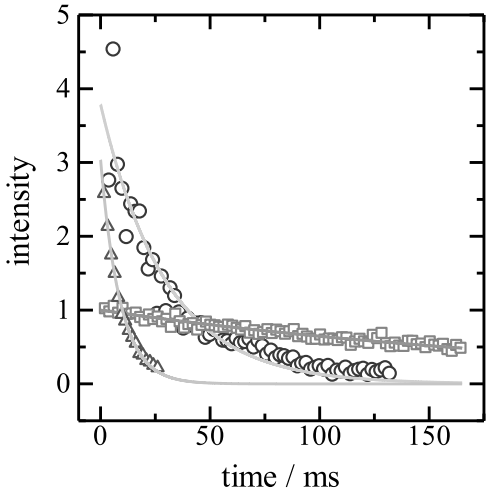

Fig. 2. Plots of the intensities of the echoes acquired by the CPMG measurement. The circles, squares and triangles express the signals from ^{1}H, ^{31}P, and ^{23}Na, respectively.

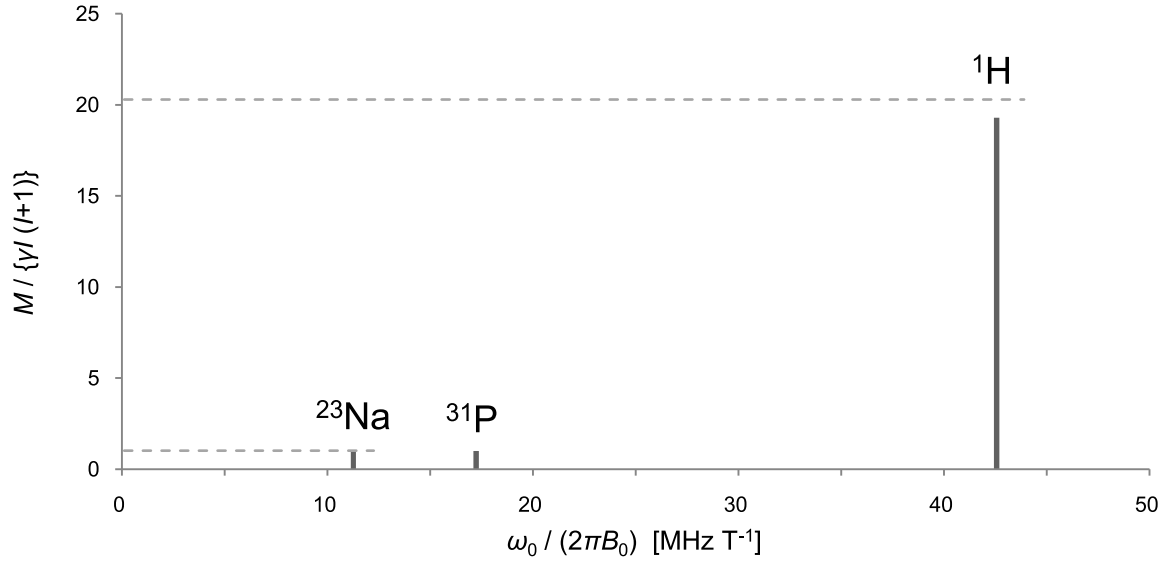

Fig. 3. A histogram of the relative abundance of ^{1}H, ^{31}P, and ^{23}Na obtained from the CPMG experiment. The data are normalized by the abundance of the ^{31}P spins. Horizontal broken lines indicates the numbers of the ^{1}H and ^{23}Na spins predicted from the amount of solute and solvent used for sample preparation.

NMR elemental analysis can be applied in principle to not only solutions but also solid-state samples. In addition, our probe is equipped with a spinning module. Currently, we are carrying out NMR elemental analysis of solid samples under magic angle spinning (MAS). The result and quantitative consideration will be described in the poster.

5. Summary

In this work, we have shown a new approach to elemental analysis using NMR, which allows one to access information as to the existence of atomic nuclei possessing spin. This work can complement other approaches for identifying isotopes through their mass and radioactivity. Furthermore, quantitative comparison between different spin species in a sample is possible, as was predicted in the principle section. The CPMG method can improve the accuracy, even if a slight error may still persist.

Acknowledgements

This work has been supported by the SENTAN program of Japan Science and Technology Agency.

References

[1] K. Takeda, *Rev. Sci. Instrum.*, **78**, 033103 (2007).
[2] K. Takeda, *J. Magn. Reson.*, **192**, 218-229 (2008).
[3] A. C. Kunwar, G. L. Turner and E. Oldfield, *J. Magn. Reson.*, **69**, 124-127 (1986).
[4] G. C. Carter, L. H. Bennett and D. J. Kahan, *Metallic Shifts in NMR, Pt. 1*, Pergamon Press.

P-146 Narrowbore HFXY Quad-resonance Probe for Solid State NMR

Jun Ashida
Agilent Technologies Japan Ltd.

All solid-state NMR experiments rely on high RF power, in order to obtain short pulse widths and high decoupling field strength. The recent trend toward high-field magnets, with higher-frequency probes, along with the need for high RF power has created a technical challenge for probe design, which in the past has required physically large capacitors to be positioned in the magnet bore next to the sample. At the same time, the high cost of high-field magnets has put a premium on bore size. The solution to this problem has been Varian's (now Agilent) innovative Transmission Tuning Tube (T3) technology. This design is more efficient and compact at higher frequency, where power and space are at a premium. Replacing the tune and match capacitors with a transmission line moves bulky components outside of valuable bore space and improves efficiency. Broadband tuning is achieved by interchanging tuning tubes, each tunable over a range of frequencies. Multiple channels are achieved with multiple tubes, which are each long and narrow to fit in a narrow bore.

This presentation illustrates several solid-state applications using the our innovative HFX(Y) Quad-Resonance Narrowbore (NB) Probe, which can handle HX, FX, HF, HFX, and HFXY experiments, without changing probes. As with all recent our solids probes, the new HFX(Y) probe uses Transmission Tuning Tube (T3) technology to obtain multiple channels in a narrowbore diameter and deliver quad-resonance ^{19}F spectroscopy to narrowbore magnets for the first time.

【Probe】

The existing our HFX(Y) widebore probe has 4 ports for H / F / X / Y, individually. The H port is for ^{1}H, F is ^{19}F, X is ^{13}C - ^{31}P and Y is ^{15}N-^{13}C. For the narrowbore HFX(Y) probe, H and F are combined into one port, using a new "Split" capability which enables dual tuning of the highband port. The HFX(Y) probe therefore requires only 3 ports (H, F / X / Y), providing four-nucleus capability in the limited diameter of the narrowbore probe. The highband tuning tube has three knobs, "Tune", "Match", and "Split" (Figure 1) to provide tuning of H and F. The Split knob changes the frequency separation between the H and the F tuning dips. The Tune and Match knobs affect both dips together.

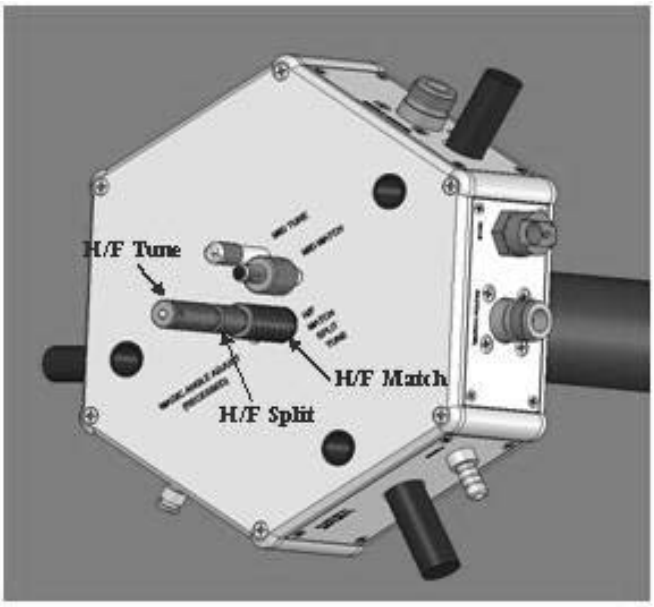

Figure 1. Location of the Tune, Match and Split knobs on the HFXY probe.

Solid State NMR, probe, Quad-resonance HFXY

As with the HX(Y) probe, which can be converted to HX, the Y channel of the HFX(Y) probe is removable to produce an HFX tuning configuration with better signal-to-noise. As with any T3 probe, the HFX(Y) probe can also accommodate the addition of our Low-gamma Box to tune nuclei below ^{15}N. The HFX(Y) probe is a versatile probe for many experiments, whether or not they involve ^{19}F.

【Application – Polymer】

Fluoropolymers are widely used for microelectronic devices, because they display excellent properties such as high thermal stability and good resistance to organic solvents. Polyvinylidene fluoride (PVDF) is one of the most common fluoropolymers.

Figure 2 shows ^{19}F/^{1}H cross-polarization magic-angle spinning (CPMAS) spectra and ^{19}F direct-polarization magic-angle spinning (DPMAS) spectra of PVDF. Normally polymers contain crystalline and amorphous regions, and how they mix determines the character of the material. It is well known that the crystalline region is emphasized by CPMAS spectra because of the strong dipolar coupling. Therefore, by comparison of CPMAS and DPMAS, crystalline and amorphous regions in the polymer can be distinguished easily. Comparison of the ^{19}F-DPMAS and ^{19}F/^{1}H-CPMAS spectra in Figure 4 illustrates that the peaks at -90 ppm and -135 ppm are in the amorphous regions, and the -70 ppm and -100 ppm peaks are in crystal regions.

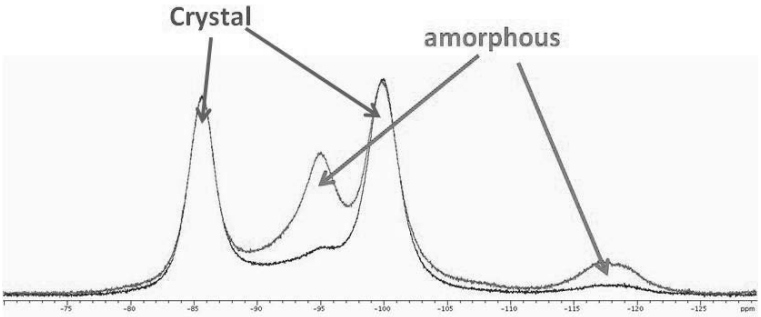

Figure 2. ^{19}F-DPMAS and ^{19}F/^{1}H-CPMAS spectra of PVDF, showing the presence of crystalline and amorphous regions.
Sample spinning speed was 37 kHz.

Figure 3 shows ^{13}C/^{1}H-CPMAS and ^{13}C/^{19}F-CPMAS spectra, which were observed with both ^{1}H and ^{19}F decoupling. These spectra demonstrate that signals for ^{13}C that are close to ^{1}H or ^{19}F are easily assigned by observing the ^{13}C signal under high resolution using simultaneous {^{1}H, ^{19}F} decoupling. If the probe was not double-tuned for ^{1}H and ^{19}F, only one of the two nuclei could be decoupled at a time, making it very hard to obtain high resolution spectra.

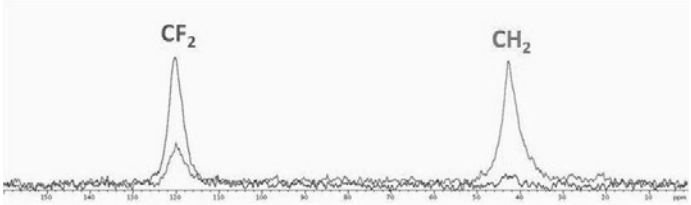

Figure 3. ^{13}C/^{1}H-CPMAS and ^{13}C/^{19}F-CPMAS spectra of PVDF. Sample spinning speed was 37 kHz. A contact time of 100 μsec was applied in order to obtain only the proton or fluorine directly coupled carbon spectrum.

Other applications will be also presented at the poster session.

P-147 Cryocoil MAS with the closed-cycle refrigerating system

Takashi Mizuno[1,3], Yasuto Noda[2,3] and K. Takegoshi[2,3]
[1]JEOL RESONANCE Inc.,
[2]Dept. of Chemistry, Graduate School of Science, Kyoto University, and
[3]SENTAN/JST

ABSTRACT

Cryocoil MAS, one of the methods to improve sensitivity of solid-state high-resolution NMR, enables us to provide an enhanced sensitivity by reducting thermal noise in the detection system insulated from a spinning sample under room temperature. Based on this guideline, we had already developed the key technologies and examined enhancement factor of ca. 4.0 was attained by two prototypes. We're going to report up-to-date development of new prototype, that is, the closed-cycle refrigerating system in consideration of general use, a special configuration for efficient cryo-cooling with ^{1}H-^{13}C double resonance circuit for 7 Tesla wide-bore SCM.

Recently, we developed a cryocoil MAS probe, with the detection acoil cryogenicly cooled at <20 K and the pre-amplifier <40 K while the sample is kept at room temperature. The S/N enhancement factor achieved so far is ca. 3 to 4 times compared with the S/N of the conventional probe.[1,2] With using the cryocoil MAS probe, we demonstrated its long-term stability by measuring ^{6}Li-^{6}Li 2D exchange NMR of $^{6}LiCoO_2$.[3] It took ca. 12 hours to observe one 2D spectrum under 7 Tesla magnet. It was shown that no appreciable t_1 noise appears, showing that the temperature of coil is stable enough to perform 2D experiments. For all measuring these preliminary experiments, we used the open-cycle refrigerating system which requires 3 to 4 liter of liquid helium per hour.

Open-cycle means direct heat-exchange with flowing liquid helium within the vacuum chamber of the cryocoil MAS probe. The liquid helium is vapored at heat-exchanger and cools the attached detection coil. The vapored helium gas is far heat exchanged with the heat-radiation shield and the attached pre-amplifier at ca. 30K before exhausted outside. This system took advantage of convenient setting for

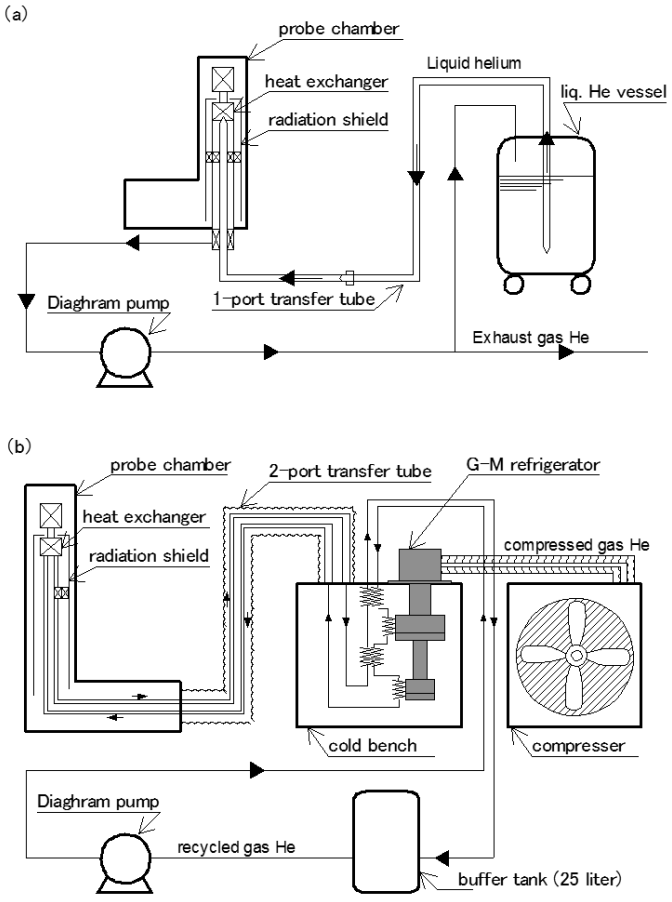

Fig.1 Schematic view of (a) open-cycle and (b) closed-cycle refrigerating system for Cryocoil MAS Probe. Arrows indicate flowing direction of coolant.

experiment without pre-cooling by liquid nitrogen, but, in the long-term machine time over ca. 1-2 days, it had a little troublesomeness to pause submitting the NMR experiment <1 hour to exchange the helium vessels of 100 liter, and the consumption of much liters of liquid helium also costs. Since 2010, we have started the development of cryocoil MAS probe for practical use. At first, we targeted the improvement of refrigerating system as user-friendly and general use.

In this work, we present a new cryocoil MAS probe with the closed-cycle refrigerating system. Closed-cycle means recycling of probe coolant. Instead of a helium vessel, we provide one type of 1.5W-4.2K Gifford-McMahon refrigerator (Sumitomo Heavy Industries Ltd.), through which the helium gas is heat-exchanged from room temperature to its vapor-point temperature, and is transmitted into the probe chamber. Thus, the main feature of our system is deprivation of two circulating lines: 1) G-M refrigerator line with highly compressed helium gas (<2.3 MPa), 2) Probe coolant line with softly compressed helium gas (<50 kPa). This system takes advantage of not only leaving the cryocoil MAS probe free from machine vibration due to high-pressure compressed gas, but also the view point of maintenance.

The performance of cooling speed is shown in Fig.2. It took about 6 hours to lead the total detection system into thermal equilibrium. The coil temperature of the new probe experimentally attained was ca.16 K, the temperature of preamplifier stage of 35 K, which matches those attained by the probe with the open-cycle refrigerating system. We are aiming to report the RF performance and S/N enhancement of NMR experiments.

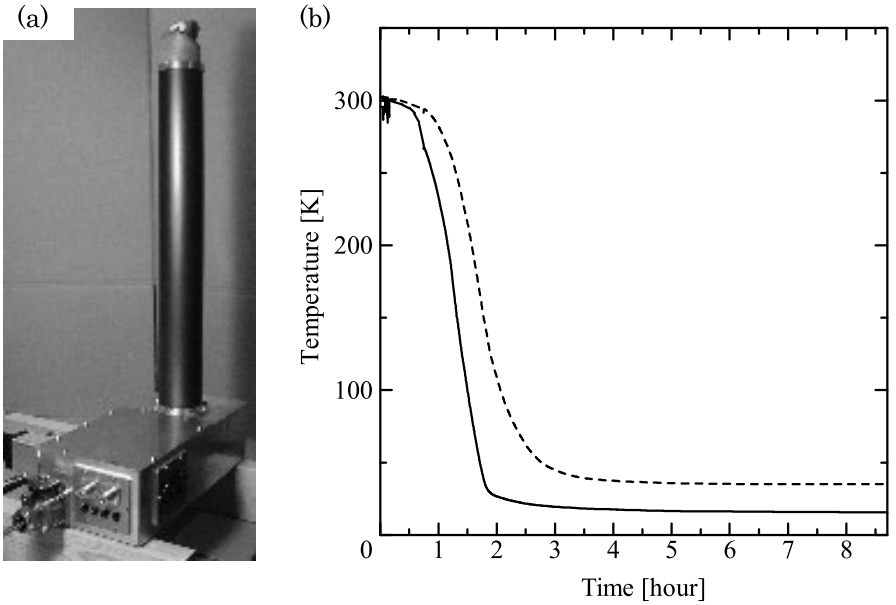

Fig. 2 New prototype of cryocoil MAS with the closed-cycle refrigerating system. (a)Photo: Probe chamber with 300 MHz ^{1}H-^{13}C double resonance circuit for 5mm spinner system.
(b) Temperature vs. time series data for each points of detection system. Solid line: the detection coil, Dashed line: preamplifier stage.

Acknowledgement: This work is financially supported by SENTAN/JST.

References [1] T. Mizuno et al., Review of Scientific Instruments 79, 044706 (2008), [2] T. Mizuno et al., Rev. Sci. Instrum. 80, 124702 (2009), [3] K. Takegoshi, "Sensitivity Enhancement by Cryo-coil MAS and Others", 52nd ENC, Asilomar CA, USA (2011)

Keywords: Cryocoil MAS, solid-state, S/N

P-149 Characterization of cellulosic supramolecular structures using solid- and solution-state NMR with stable isotope labeling

Tatsuki Ogura[1], Yasuhiro Date[1, 2], Yuuri Tsuboi[3], Jun Kikuchi[1, 2, 4, 5]

[1]Grad. Sch.Nanobio., Yokohama City Univ., [2]RIKEN Plant Sci. Cent. [3]RIKEN Adv.Sci. Inst., [4]Grad. Sch. Bioagri., Nagoya Univ., [5]Biomass Eng. Prog., RIKEN Res. Clust. Innov.

Abstract

Macromolecular complex such as lignocellulose, which is major component of plant cell walls, plays many roles of providing physical and biological strength of plants, namely against microbial attack. However, little information about the biomass supramolecular structure is available. Therefore, this study focused on the characterization of the biomass supramolecular structure by using solid- and solution-state NMR such as CP/MAS, HETCOR, and HSQC with stable isotope labeling.

Introduction

Lignocellulose, which is major component of plant biomass and persistent substances forms complex composed of cellulose, hemicellulose, and lignin. It plays many roles of providing physical and biological strength of plants, namely against microbial attack[1-3].

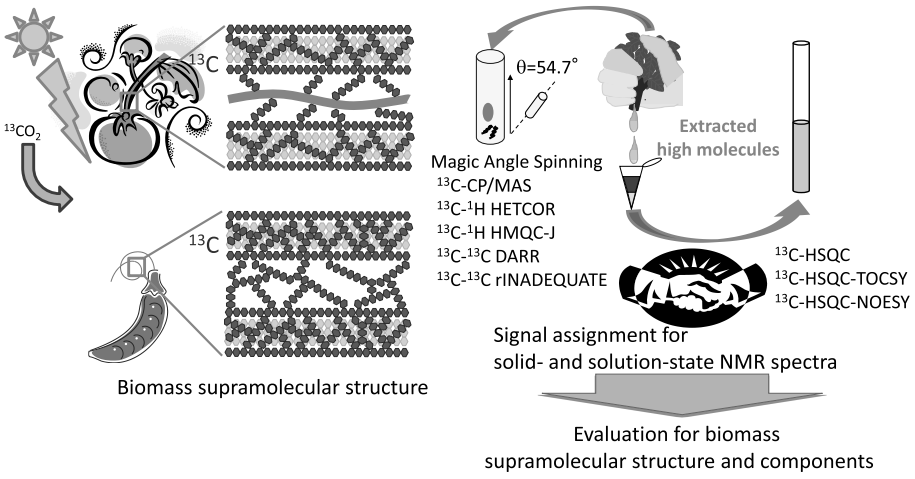

Fig. 1 Analytical strategy for biomass supramolecular structure and components

In recent studies, biomass components such as lignin and hemicellulose were characterized by ^{1}H-^{13}C HSQC NMR spectra with DMSO/pyridine solvent system[4]. However, little information about biomass supranolecular structure and chemical linkage between their components is available. Therefore, we are now attempting to elucidate the biomass supramolecular structure and their components using solid- and solution-state NMR such as CP/MAS, HETCOR, and HSQC (Fig. 1). In this study, the compositional variations and chemical linkage between biomass components in plant biomass were evaluated using ^{13}C-labeled biomass.

Biomass, Stable isotope labeling, Supramolecular structure

Methods

We made ^{13}C-labeled biomass samples such as haulm of soybean, haulm of tomato, and leaf of komatsuna (Japanese Mustard Spinach). These samples were freeze-dried and gently processed using food cutter and Auto milling machine. These samples were measured by solid-state NMR such as CP/MAS and HETCOR to analyze supramolecular structures. In addition, small-molecules were removed from milled biomass samples using H_2O and MeOH. These residual macromolecular fractions were treated by Hexafluoroacetone (HFA) to remove protein. Treated samples were processed by ball-milling and then dissolved using DMSO-d_6/pyridine-d_5. The samples were measured by solution-state NMR such as ^{1}H-^{13}C HSQC and ^{1}H-^{13}C HSQC-TOCSY.

Results and Discussion

^{13}C-labeled biomass samples treated by Auto milling were analyzed by solid-state NMR spectroscopy to evaluate biomass supramolecular structure. Some specific peaks in ^{13}C-labeled samples were detected in CP/MAS analysis (Fig. 2a-d), whereas certain peaks were not detected in non-labeled samples. In addition, to identify these peaks, ligunocellulosic components in ^{13}C-labeled biomass samples were analyzed using ^{1}H-^{13}C HSQC spectra (Fig. 2e, f) and assigned by Bm-Char tool (URL; https://database.riken.jp/ecomics/biomass/). Some peaks detected in HSQC spectra were identified as lignocellulosic components. This result was consistent with the obtained peaks at CP/MAS spectra. Therefore, multiple analyses of solid- and solution-state NMR spectra may have a potential to determine biomass supramolecular structure. In this symposium, we will discuss more detailed information about biomass supramolecular structure using solid- and solution-state NMR spectroscopy.

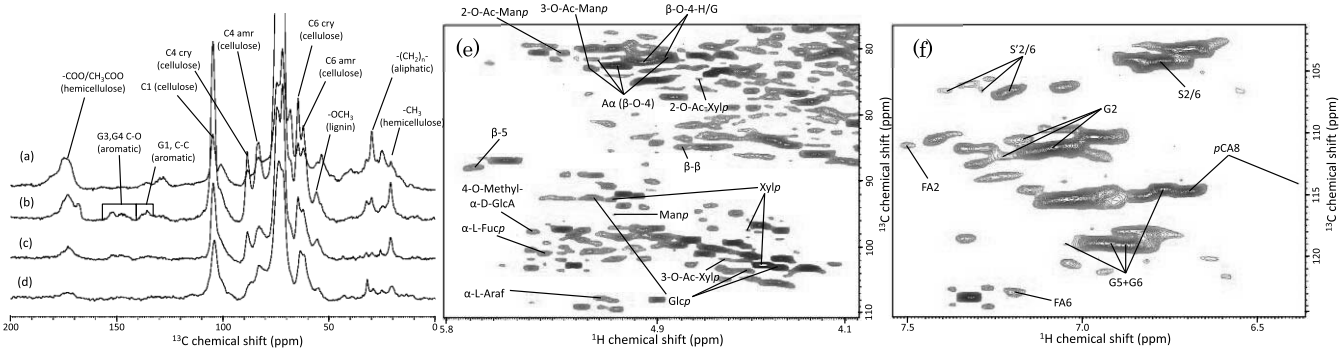

Fig. 2 Evaluated ^{13}C-labeled and non-labeled biomass supramolecular structure (a-d), and biomass components (e-f). (a) CP/MAS spectra of ^{13}C-labeled komatsuna, (b) ^{13}C-labeled tomato, (c) ^{13}C-labeled soybean, (d) non-labeled rice, (e) HSQC spectra of lignin side chain and polysaccharide region, and (f) lignin aromatic region.

Reference

(1) Jing Ke, Dhrubojyoti Dey Lasker, and Shulin Chen, *Biomacromolecules*, 2011, **12**, 1610-1620

(2) Purbasha Sarker, Elena Bosneaga and Manfred Auer, *J. Exp.Bot*., 2009, **60**, 3615-3635

(3) Joseph B. Binder and Ronald T. Raines, PNAS., 2010, **107**, 4516-4521

(4)Hoon Kim and John Ralph, *Org. Biomol. Chem.*, 2010, **8**, 576-591

P-150 Evaluation the mobility of rubber molecules exposed to high-pressure hydrogen gas

Hiroaki Ono[1], Hirotada Fujiwara[2] , Jyunichiro Yamabe[2,3] , Shin Nishimura[2,4]
[1] School of Engineering, Kyushu University (Japan)
[2] The Research Center for Hydrogen Industrial Use and Storage, AIST (Japan)
[3] International Research Center for Hydrogen Energy, Kyusyu University (Japan)
[4] Department Mechanical Engineering, Faculty of Engineering, Kyusyu University (Japan)

Abstract

In order to clarify the performance and durability of high-pressure hydrogen sealing rubber materials, it is important to evaluate their molecular mobility. We have evaluated the time dependency of the molecular mobility of acrylonitrile-butadiene rubber (NBR) by using pulsed NMR. Hydrogen content and hydrogen release profile of the same samples were measured in terms of thermal desorption analyses. We will discuss the relationship between molecular mobility and hydrogen desorption behavior of rubber materials.

Introduction

Recently, the hydrogen energy is paid to attention as one of the clean energy instead of the fossil fuel, and practical use is advanced. The rubber materials for high-pressure hydrogen, for example using by sealing material of high-pressure hydrogen gas vessel, are required high sealing property and high durability. However, the explosive decompression failure of the rubber material for sealing using in general exposed to high-pressure hydrogen has been reported[1]. This phenomenon is caused by hydrogen dissolved in the rubber materials. Therefore, the consideration for effect of the hydrogen on the rubber materials can be important information for understanding the blister fracture.

In this study, for evaluating the effect of the hydrogen gas on the rubber material, the time dependency of T_2, the spin-spin relaxation time of NBR exposed to 100 MPa hydrogen gas after the decompression was measured by pulsed NMR method, and of the hydrogen content was measured by thermal desorption gas analysis.

Experimental

The NBR samples of the acrylonitrile content 18%(NBR18) and 33.5% (NBR33.5) were used. The size of samples were ϕ6 mm $\times$13 mm cylinder. The samples were exposed to 100 MPa hydrogen. After decompression, the spin-spin relaxation time (T_2) of the samples was measured by pulsed NMR (Bruker, The minispec mq20) using the condition shown in Tab.1, and the hydrogen component measured by thermal desorption gas analysis (TDA) (J・Science Lab, GIF20A). These measurements were condercted in the same temperature at 30℃.

pulsed NMR , rubber, high pressure hydrogen

Tab.1 The experimental Condition of the pulsed NMR

Equipment	Bruker, The minispec mq20
Resonant frequency【MHz】	19.65
Pulse sequence	Solid echo (90° x - 90° y)
90° pulse length【μs】	2.76
Recycle Delay【s】	0.5
Separation between 90° pulse【ms】	0.001
Fitting function	$Y = A_1 * exp(-x/\tau_1) + A_2 * exp(-x/\tau_2)$
	A_1, A_2: amplitudes of components 1 and 2 at time zero
	τ_1, τ_2: T2 decay constants of components 1 and 2

Results and discussion

Hydrogen content and T_2 of NBR33.5 and NBR18 with elapsed time were shown Fig.1. The FID signal of NBR33.5 could be fitted to 2 components, but NBR18 could not be done. So, we compared with T2 of NBR18 and T2 total ($=(A_1/(A_1+A_2)*\tau 1+A_2/(A_1+A_2)*\tau_2$) of NBR33.5. The T_2 and T_2total of soon after decompression were shorter than that of before exposed samples, and increased as time elapsed. And the T_2 of NBR33.5 and NBR18 were return to the value of before exposure samples at about 3000 minutes and about 1500 minutes. On the other hands, those results corresponded almost to T_2 increasing behavior.

From above results, ① the molecular mobility became lower by hydrogen exposure ② the degree of the inhabitation was different by acrylonitrile content, were suggested.

We are planning to measure the pulsed NMR of NBR sample containing 50% of acrylonitrile. We will discuss about the effect of the acrylonitrile content on the relaxation process of the NBR.

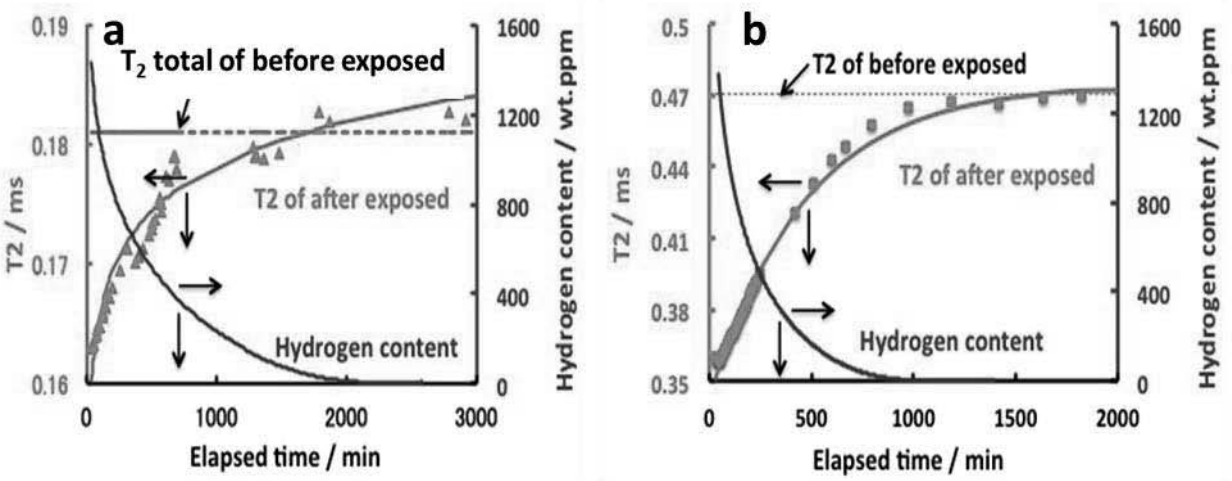

Fig.1 The time dependency of T_2 and hydrogen content of a) NBR33.5 and b) NBR18

Reference

1. J. Yamabe and S. Nishimura, *International Journal of Hydrogen Energy*, *34*, 1977 （**2009**）

Acknowledgement

This research has been supported by the New Energy and Industrial Technology Development Organization (NEDO) "Fundamental Research Project on Advanced Hydrogen Science (2006-2012)".

P-151 Comparative metabolomics of compositional variations and diversities in plant biomass from hydrosphere

Kenji Sakata[1], Yasuhiro Date[1,2] and Jun Kikuchi[1,2,3,4]

[1] Graduate School of Nanobioscience, Yokohama City University
[2] RIKEN Plant Science Center
[3]Biomass Engineering Program, RIKEN Research Cluster for Innovation
[4]Graduate School of Bioagricultural Sciences, Nagoya University

NMR-based metabolomics approach has been used extensively to study metabolites in a wide range of biological systems. Although these approaches are powerful tools for evaluation of low-molecular compounds, some scientists in next step face a significant challenge for characterization of the complex plant biomass. In this study, we focused on the characterization and comparisons for plant biomass from hydrosphere. The compositional variations and diversities in plant biomass were evaluated by NMR-based metabolomics and other physicochemical approaches with multivariate statistical analysis.

[Introduction]

NMR-based metabolomics approach has been used extensively to study metabolites in a wide range of biological systems such as plants, animals, and microbial ecosystems (1-4). This approach has flexibility and applicability for combination with other methods, thus we previously reported to develop an approach in combination of the metabolomics with microbial community analysis for monitoring the metabolic dynamics in microbial ecosystems and linking the relationships between microbial community and their metabolic information (1). Although these approaches are powerful tools for evaluation of low-molecular compounds such as short-chain fatty acids and amino acids, some scientists in next step face a significant challenge for evaluation and characterization of the complex biomacromolecules (e.g. plant biomass and polysaccharide in seaweed). To address this challenge, we are now attempting to develop an approach to characterize the compositional variations and diversities of polysaccharides in intertidal seaweeds for evaluation of the complex biomacromolecules in natural ecosystems. In this study, comparative analysis of diversed intertidal seaweeds were evaluated by the NMR-based metabolomics approach, element profiles characterized by Inductively Coupled Plasma-Optical Emission Spectrometry/Mass Spectrometry(ICP-OES/MS), and other physicochemical approaches with multivariate statistical analysis.

[Materials and Methods]

The hydrosphere biomass used in this study was collected from Aburatsubo and Tenjinjima in Kanagawa, Japan. The collected samples classified into brown, green, and red algae were freeze-dried, crashed, and processed into particle size by using ball-mill and Automill machines. The samples processed by Automill machine were measured by Fourier transforms infrared (FT-IR), ICP-OES/MS, and thermogravimetric-differential thermal analysis (TG-DTA) instruments. The ball milling samples were suspended in deuterium oxide (D_2O) with 1 mM sodium 2,2-dimethyl-2-silapentane-5-sulfonate (DSS) as an internal standard to measure by NMR spectroscopy.

Keywords: comparative metabolomics/ plant biomass/ physicochemical approach

After exclusion of water resonance, each region was integrated and normalized to the total of DSS integral regions. Each data including ^{1}H NMR, FT-IR, and ICP-OES/MS were processed by binning, digitizing, and evaluating with multivariate statistical analysis such as principal components analysis (PCA). In this study, PCA visualized as score plots was run in the 'R' software.

[Results and Discussion]

To mine the information of individual characteristics in natural algae samples, the compositional variations and diversities in plant biomass were evaluated by NMR-based metabolomics and other physicochemical approaches with multivariate statistical analysis based on the sampling procedures in figure 1. By PCA score plots of ^{1}H NMR, FT-IR, and ICP-OES data matrices, the metabolomic, ionomic, and biomass profiles in intertidal seaweeds were likely to cluster according to the differences of the taxonomic groups (i.e. green, red, and brown algae). Therefore, our sampling procedures were capable of mining the information of individual characteristics in diversed algae biomass.

In addition, the relationships between metabolic compositions and elemental profiles in intertidal seaweeds were found by the metabolome-ionome correlation analysis. These approaches will provide a platform technology for evaluating the compositional variations and diversities of plant biomass from hydrosphere and opening a new avenue that will clarify the complex biomacromolecules in natural ecosystems.

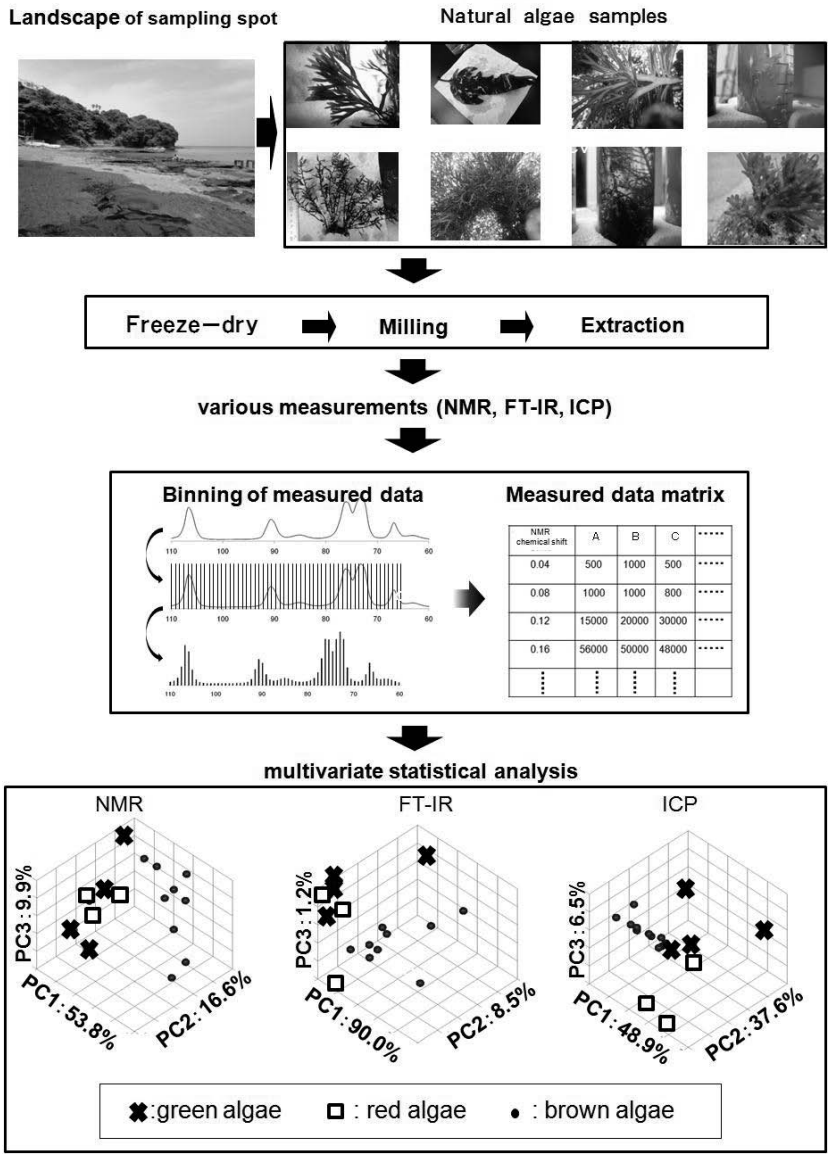

Figure 1. Sampling procedures and methodological flows for evaluation of the compositional variations and diversities in plant biomass from hydrosphere.

[References]

(1) Date Y. et al. ***J. Biosci. Bioeng***. (2010)**110**, 87-93.
(2) Fukuda S. et al. ***Nature*** (2011)**469**, 543-547.
(3) Nakanishi Y. et al. ***J. Proteome Res***. (2011)**10**, 824-836.
(4) Sekiyama Y. et al. ***Anal. Chem***. (2011)**83**, 719-726.

P-153 Detection of illegal drugs by nuclear quadrupole resonance

Junichiro Shinohara[1], Bryn Baritompa[1], Hideo Sato-Akaba[1] and Hideo Itozaki[1]
[1]Graduate school of Engineering Science, Osaka University

ABSTRACT

We developed a screening device using nuclear quadrupole resonance (NQR), which is able to detect illegal drugs concealed in the human body. The device consists of an NQR spectrometer with a single spiral coil antenna. The subject person lies in the electro magnetically shielded box, and their body was scanned by the device. NQR experiments were performed using typical narcotics of methamphetamine hydrochloride. It was wrapped by meat of 35 mm thick layer to simulate the drug concealed in the body. 144g methamphetamine hydrochloride were successfully detected by 25 s.

INTRODUCTION

One of the NQR applications is the noninvasive detection of illegal drugs and explosive substances. NQR is similar to NMR in which energy gaps are generated by an external magnetic field. Nuclei with a spin of one or more have electric quadrupole moments, and their energies are split by the intrinsic electric field gradient, which is highly specific to the substance. Therefore, an additional external static field is not necessary to generate the energy gaps for NQR. An advantage of NQR in touch detection is compactness of apparatus, because the magnet is not necessary for this method.

Drug concealed in the body has rapidly increased since the September 11, 2001 terrorist attack in the U.S. because tightened security systems have made conventional smuggling difficult [1]. While external body scanning, drug sniffing dogs, and pat down searches are not useful for sensitive, scanning using NQR has potential as it uses RF fields which penetrate the body. In addition, samples concealed in the human body will be at body temperature and not possess a strong temperature drift, leading to advantageous conditions for NQR signal detection.

We developed a screening device using NQR, which is able to detect methamphetamine hydrochloride concealed in the human body. The device consists of an NQR spectrometer with a single spiral coil antenna and an electromagnetically shielded box. The subject person lies in it, and has their body scanned using the NQR body scanner.

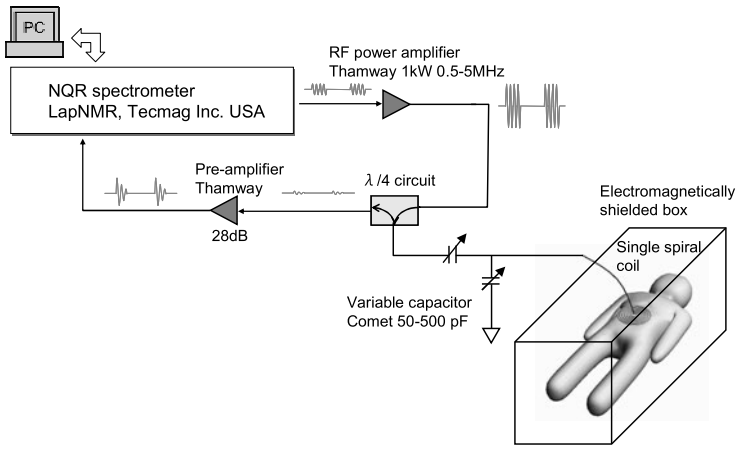

Fig. 1 Block diagram of the NQR body scanner

We have investigated an NQR signal sensitivity of methamphetamine hydrochloride in the body.

nuclear quadrupole resonance, NQR, methamphetamine hydrochloride

METHODS

The device consists of an NQR controller, RF power amplifier, λ/4 circuit, pre-amplifier and a single spiral coil antenna. The block diagram of the device is shown in Fig. 1. We made a single spiral coil 22 turns and it has antenna for a Q switch [2]. Whole size of antenna was 190 mm in outer diameter, 1 mm in thickness and made of copper. The Q factor was 190. The electromagnetically shielded box was 1.9 × 0.83 × 0.63 m, enough space for a person to lie down in. Methamphetamine hydrochloride (144 g) was wrapped by meat. The distance between the sample and the spiral coil antenna was adjusted by changing thickness of the meat layer. The coil was placed beneath the meat. To increase an NQR signal intensity, a spin-locking spin echo (SLSE) sequence was applied [3].

RESULTS AND DISCUSSION

NQR signal was observed clearly from methamphetamine hydrochloride in the simulated body using meat layer by 25 s. It is showing in Fig 2. Difference of the signal intensity was negligible with and without using the meat since the RF frequency of ~1 MHz for the excitation pulse was low enough to consider a dielectric loss in the body. The SNR was about 4 in the case of meat thickness of 14 mm. The NQR signal intensity was decreased by increasing the meat layer thickness as shown in Fig 3. The achieved sensitivity suggested that the detection of methamphetamine hydrochloride concealed in the human body is possible when it is concealed at the depth of ~ 4 cm from the surface of the body.

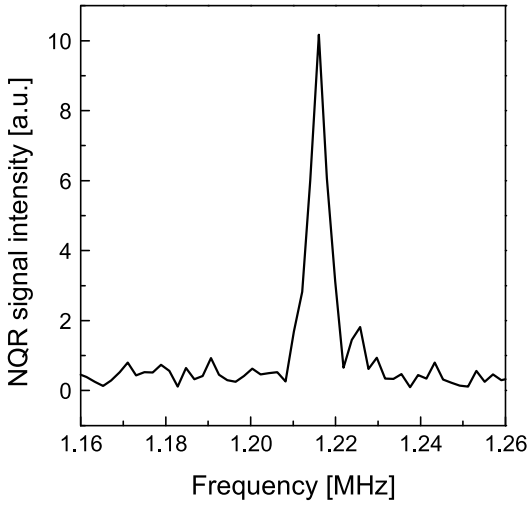

Fig. 2 NQR spectrum of methamphetamine hydrochloride obtained using a SLSE sequence. The sample was wrapped by meat with 14 mm thick.

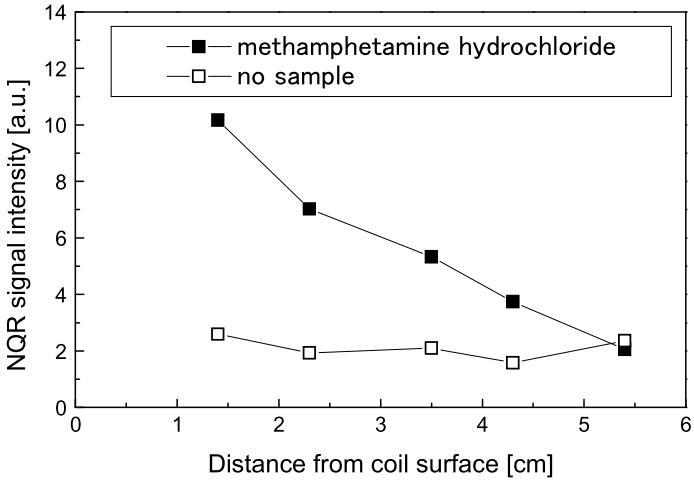

Fig. 3 Meat thickness dependence of NQR intensity.

REFERENCES

[1] K. Takekawa, T. Ohmori, A. Kido, and M. Oya, *J. Forensic Sci.,* 52 (2007) 1219-1222.
[2] E.R. Andrew, and K. Jurga, *J. Magn. Reson.* 73 (1987) 268-276.
[3] R.A. Marino, and S.M. Klainer, *J. Chem. Phys.,* 67 (1977) 3388-3389.

P-154 Accurate purity calibration of pesticides using NMR

Takeshi Saito, Yoko Ohte, Masayo Murakami, Toshihide Ihara
Chemical Measurement System Section,
Measurement Standards System Division,
National Metrology Institute of Japan, AIST

Introduction

For the analysis of pesticides in food or environmental samples, chromatographic methods such as gas chromatography and high performance liquid chromatography are conventionally used because these are easy, sensitive and applicable to the determination of multi component mixtures. One drawback to these techniques is that it requires calibration of instrument for each and every analyte of interest if accurate quantification is to be achieved. This requires high purity neat substances whose purity was certified for any given analyte to obtain reliable analytical results. Unfortunately, determination of the purity of neat substances is not an easy task. When considering the traceability to the International System of Units (SI), it is more difficult because of limited number of SI traceable analytical methods. In 2006, regulation of pesticides in food limiting the positive maximum residue (positive list system) in Japan has been brought into effect [1]. Preparation of certified reference materials (CRMs) [2] for some 800 regulated pesticides is a big challenge at the moment. Additionally, ISO/IEC 17025 requires for calibration and testing laboratories to program calibrations and measurements traceable to the SI. Demands on the CRMs has been increasing rapidly, on the other hands, production of CRMs for such objectives has still been limited because of difficulties of purity assessments. Such requirements introduce the need to implement a new approach for producing SI traceable CRMs more effectively. Although accurate absolute intensity measurements are difficult in quantitative NMR (qNMR), the area of a signal from a compound can be measured with respect to the other signal originating from the other compound. This feature makes qNMR extremely attractive for purity determinations. Therefore, this makes qNMR possible to need only one standard, or a universal standard, for the entire determinations.

Purity determination, validation and its uncertainty estimation, and traceability of qNMR

Suppose a mixture of a sample and an internal standard (IS) resonates at different chemical shifts, one can obtain signals from a spectrum independently. Under this condition, the purity of an analyte in the sample can be calculated from

$$p_{\mathrm{x}} = \frac{S_{\mathrm{a}}}{S_{\mathrm{s}}} \frac{N_{\mathrm{s}}}{N_{\mathrm{a}}} \frac{M_{\mathrm{a}}}{M_{\mathrm{s}}} \frac{m_{\mathrm{x}}}{m_{\mathrm{s}}} p_{\mathrm{s}} \qquad (1)$$

where S, N, M, m and p represent peak area, the number of ^{1}H nuclei for the peak, molecular mass, mass of the sample, and purity, respectively; subscripts a, x and s represent the analyte, the sample and the IS, respectively. Different approach to choose NMR experimental parameters is important because NMR experimental parameter sets for chemical structure determination often focus on obtaining a spectrum of best signal to noise ratio, which may not consider quantitative responses of signal intensities. By selecting the experimental parameters, validation of the experiments was checked using several CRMSs; for example, purity of one CRM, NIST SRM 350a, was analyzed by

qNMR with another CRM, NMIJ CRM 4039-a, as an internal standard.

From the equation (1), uncertainties associated to NMR experimental parameters, S and m, are not independent factors thus can be evaluated by analysis of variance. Additionally, parameter S is a function of relaxation delay and excitation pulse width and longitudinal relaxation time, T_1; the uncertainty associated to this term is also important. Uncertainties associated to molecular mass, natural abundance of ^{1}H that affects the number of ^{1}H nuclei are obtained from literature, purity of the IS are obtained from its certificate.

According to the equation (1), purity obtained by qNMR is based on the comparison of the number of nuclei, or comparison of moles. The traceability for the purity of the analyte observed by qNMR is defined clearly to the purity of the IS for the reference by SI. When SI traceable CRM is used for the IS for the qNMR experiments, the purity obtained by qNMR are traceable to the CRM, thus SI traceable result can be obtained by the method.

In this presentation, we demonstrate accurate purity calibration of pesticides using NMR. The validity and the accuracy of the of the purity analysis, the uncertainties associated to the analysis and its traceability are described.

Remarks

At National Metrology Institute of Japan (NMIJ), we have been using this technique for the calibration services of purity of organic substances. Reference materials calibrated by this service will be able to state their traceability to SI. Our traceability scheme is as shown in Figure 1. Processes that are in the rectangle are operated by NMIJ for ensuring traceability to the SI, while the reference material producers will be able to produce many different kinds of SI traceable reference materials using this scheme.

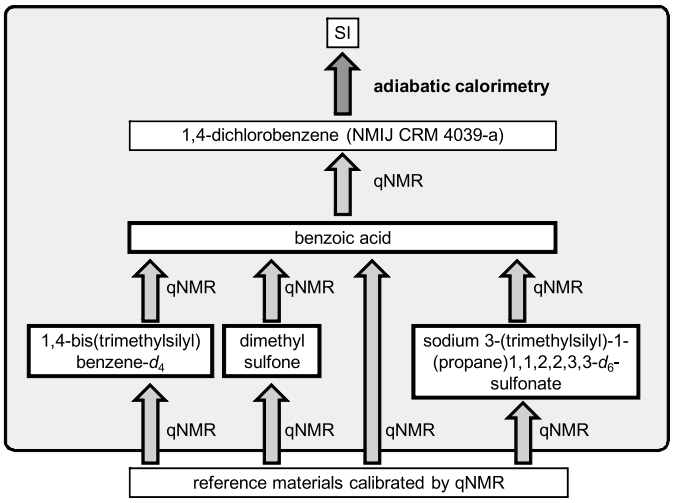

Figure 1 Traceability system for the qNMR calibration system provided by NMIJ. Compounds in bold lines are the ISs often used at NMIJ.

References

[1] Introduction of the Positive List Systems for Agricultural Chemical Residues in Food (2006) Department of Food Safety, Ministry of Health, Labor and Welfare, Tokyo, Japan. http://www.mhlw.go.jp/english/topics/foodsafety/positivelist060228/introduction.html. Accessed 1, April 2011

[2] ISO Guide 30: 1992/Amendment 1: 2008 (2008) Terms and definitions used in connection with reference materials/Amendment 1 Revision of definitions for reference material and certified reference material, ISO, Switzerland

[3] Wells RJ, Cheung J, Hook JM (2004) Accred Qual Assur 9:450–456

NMR, quantification, purity calibration, accuracy, metrological traceability, pesticide

P-155 Variable Lymphocyte Receptor (VLR), a good candidate for antibody alternatives

Byung Woo Han[1]
[1]Department of Pharmacy, Seoul National University, Korea

ABSTRACT

Variable lymphocyte receptors (VLRs) play the primary role in recognition of antigens in the adaptive immune system of jawless vertebrates. We have determined the structure of VLR RBC36 in complex with the H-antigen trisaccharide. VLR RBC36 binds the H-trisaccharide on the concave surface of the LRR modules of the solenoid structure where three key hydrophilic residues, multiple van der Waals interactions, and the highly variable insert of the LRRCT determine antigen recognition and specificity. We are trying to produce antigen specific VLRs from hagfish and the production of antigen-specific VLRs would be a foundation stone for the search of antibody alternatives.

REFERENCE

Han BW, Herrin BR, Cooper MD, & Wilson IA, “Antigen recognition by variable lymphocyte receptors” (2008) Science, 321:1834-7

Variable Lymphocyte Receptor, VLR, Antibody alternatives